Chemical Science

EDGE ARTICLE

View Article Online
View Journal | View Issue

Cite this: *Chem. Sci.*, 2014, **5**, 2554

Aqueous solubilization of hydrophobic supramolecular metal–organic nanocapsules†

H. Kumari,[a] S. R. Kline[b] and J. L. Atwood*[a]

Received 5th January 2014
Accepted 25th February 2014

DOI: 10.1039/c4sc00035h

www.rsc.org/chemicalscience

Micelles of metal-seamed *C*-propylpyrogallol[4]arene-based [$(PgC_3)_nM_{4n}L_{0-4n}$, L = ligand, M = metal] hexamers and dimers in water have been formulated using non-ionic surfactants and characterized using *in situ* scattering techniques. Polysorbitans (tween 20, tween 40, tween 80) are utilized to solubilize $(PgC_3)_6Cu_{24}$ and $(PgC_3)_6Ni_{24}L_{24}$ hexamers, $(PgC_3)_2Ni_8L_8$, $(PgC_3)_2Zn_8L_8$, and $(PgC_3)_2Co_8L_8$ dimers in water. The dimensions of micelles of tweens⊂$(PgC_3)_nM_{4n}L_{0-4n}$ dimers and hexamers are studied using dynamic light scattering (DLS; hydrodynamic radius/R_h) and small-angle neutron scattering (SANS). SANS data is fitted to a polydisperse core–shell–sphere model (static radius/R_{HS}) and used to calculate the radius of gyration (R_g). An increase in radius of the tween 20 (C12)- and tween 40 (C16)-based micelles is observed with an increase in the radius of the nanocapsule (dimer *vs.* hexamer); however, given the longer alkyl tails of tween 80 (C18:1, *cis*-9), a progression in radius is not observed for tween 80-enclosed micelles due to the unsaturation (C9) and bent alkyl tail of the surfactant. The R_g : R_h ratios are close to 0.77 for the control (0.62), tween 20⊂dimeric (0.67) and tween 20⊂hexameric (0.68) micelles that demonstrates the sphericity of micelles in water. In contrast, the higher R_g/R_h ratio (0.76 to 0.93) of tween 80-based micelles is indicative of more elongated micellar species in aqueous solution.

Introduction

The design of supramolecular complexes with surfactants, such as sodium dodecyl sulfate with poly(amido amine)/PAMAM dendrimers,[1] *n*-octyltrimethyl ammonium hexafluorophosphate with pillar[*n*]arenes[2–4] and cetyltriethylammonium bromide (CTAB) with *p*-sulfonatedcalix[4,6]arene[5] or the synthesis of polymer–surfactant based systems, such as crown-ether based polymer,[6] pluronic-CTAB or pluronic F88-CTAC (cetyl-triethyl ammonium chloride) block copolymers, is often intriguing.[7–9] The design of such complex architectures is difficult; however, tailoring their architectures for modified chemical and physical properties is even more challenging. One can introduce structural modifications into these systems as a function of surfactant, probe or co-surfactant concentration. Such alterations in structural properties can then be studied using time-resolved fluorescence anisotropy, small-angle neutron scattering (SANS) or dynamic shift measurements.[7–9] The structural properties of surfactant-based complexes are interesting because of their varied applications in industrial and material science. For example, calixarene-based nanoemulsions (a) aid in the extraction of uranium from contaminated solutions,[10] (b) selectively extract membrane proteins[11] and (c) form artificial transmembrane ion-channels.[12]

Inspired by the huge possibilities of practical applications, we identified metal-seamed pyrogallol[4]arene- (PgC_nM, where *n* is the alkyl tail length and M is metal) based nanocapsules as suitable candidates for co-complexing with surfactants.[13–17] The encapsulation sites available within these PgC_nM-based nanocapsules render them captivating candidates for practical applications such as drug delivery.[13,18–22] These macrocycles, PgCs, have been shown to encapsulate several flourophore probes, such as pyrene, pyrene butanol, ADMA, pentacene and acanapthene.[18–22] Structurally similar to PgC_n, resorcin[4]arenes (RsC_n) have also been shown to encapsulate insulin monomer as a guest moiety.[23]

Although significant efforts have been directed towards the synthesis[24] and encapsulation[18] of metal-seamed organic nanocapsules (MONCs),[25–32] their stability in solution has been less explored. Previous studies have shown the formation of MONCs in various organic solvents.[24] Specifically, the formation of pyridine-coordinated zinc-seamed *C*-alkylpyrogallol[4]arene/$(PgC_n)_2Zn_8$ dimeric capsules in dimethylsulfoxide/DMSO or copper-seamed *C*-alkylpyrogallol[4]arene/$(PgC_n)_6Cu_{24}$ hexameric capsules in acetone or methanol.[24] Each dimeric and hexameric nanocapsule is composed of two and six pyrogallol[4]arene units, respectively, with 4 : 1 metal to pyrogallol[4]arene ratio. The dimers [$(PgC_n)_2Zn_8L_8$, $(PgC_n)_2Co_8L_{8-10}$, $(PgC_n)_2Ni_8L_8$]

[a]*Department of Chemistry, University of Missouri-Columbia, 601 S. College Avenue, Columbia, MO 65211, USA. E-mail: AtwoodJ@missouri*

[b]*NIST Center for Neutron Research, National Institute of Standards and Technology, 100 Bureau Drive, Stop 6102, Gaithersburg, MD 20899, USA*

† Electronic supplementary information (ESI) available. See DOI: 10.1039/c4sc00035h

have pentacoordinated metal centers with external ligands/L (pyridine or DMSO) whereas the hexamers may ($(PgC_n)_6Ni_{24}L_{24}$) or may not ($(PgC_n)_6Cu_{24}$) have external ligands on their metal centers, confirmed by single-crystal X-ray diffraction studies (Fig. 1).[24]

These capsules, in particular dimers, have shown ligand exchange and encapsulation of protonated guests without compromising the host framework. More recently we have demonstrated the solution stability of these hexameric (R = 10 Å) and dimeric (R = 7 Å (without ligand) / 9 Å (with ligand)) nanocapsules in solvents such as methanol, acetone and DMSO.[33–35]

Notably, the metal-seamed pyrogallol[4]arenes are insoluble in water except those with C1 alkyl tails, which restrains their practical applications and bioavailability. The aqueous solubilzation of these nanoassemblies *via* surfactants, can potentially aid in making macrocycles more bioavailable. The current study focuses on the solubilization of these metal-seamed organic nanocapsules (MONCs) in water using non-ionic surfactants. Specifically, we make stable solutions of $(PgC_n)_6Cu_{24}$ (without external metal-coordinated ligands) hexamer, $(PgC_n)_6Ni_{24}L_{24}$ (with external metal-coordinated ligands) hexamer and $(PgC_n)_2Ni_8L_8$ dimer, $(PgC_n)_2Co_8L_8$ dimer and $(PgC_n)_2Zn_8L_8$ dimer in water using non-ionic surfactants, namely tweens (polysorbitans). The solution structures of these micellar complexes are investigated using dynamic light scattering (DLS) and small-angle neutron scattering (SANS). Also, appropriate comparisons/conclusions are drawn between the dimensions of micelles obtained from the two techniques. To our knowledge, this is the first study on aqueous solubilization of metal-seamed pyrogallol[4]arenes.

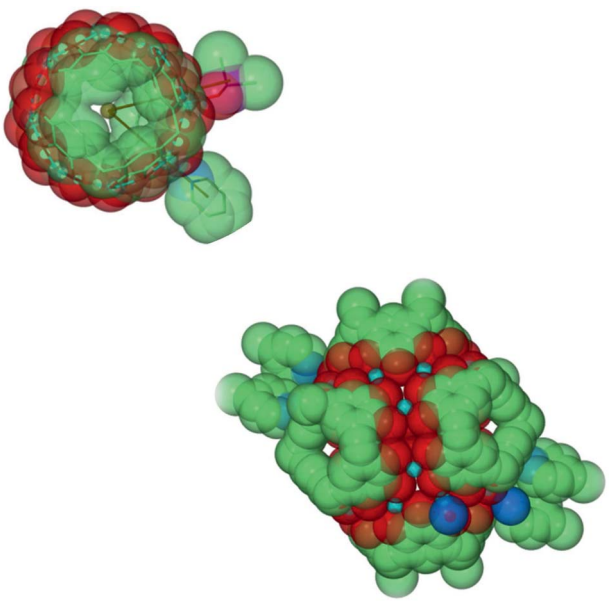

Fig. 1 The top view of a metal-seamed pyrogallol[4]arene based dimer with external metal-coordination ligands (DMSO/pyridine) showing the overall increase in diameter of capsule with ligands (top left). The front view of a metal-seamed pyrogallol[4]arene based hexamer with four external pyridine ligand (bottom right). Space filling representations are shown to illustrate the size of spheres. Colour codes: C: green; O: red; M: turqouise; N: blue.

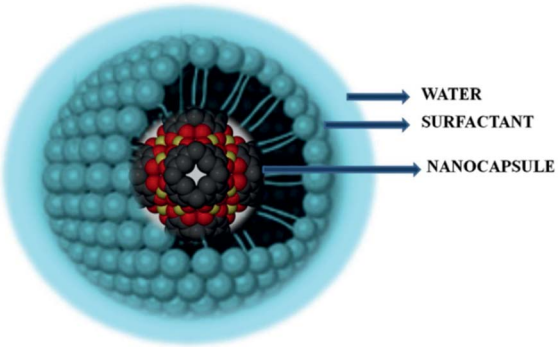

Fig. 2 Space-filling representation of the surfactant solubilised hexameric *C*-alkylpyrogallol[4]arene nanocapsule.

Results and discussion

A uniform dispersions of $(PgC_3)_6Cu_{24}$ hexameric, $(PgC_3)_2Ni_8L_8$ and $(PgC_3)_2Zn_8L_8$ dimeric micelles in water were prepared by the aid of a surfactant–cosurfactant mixture. The surfactants reduced the interfacial tension between the hydrophobic capsular surface and the hydrophilic aqueous phase. The type of non-ionic surfactant for solubilization was chosen based on the calculated hydrophilicity index (HLB) values. A broad range of solubility index was tested for optimization with hydrophobic (span 80: HLB value 4.3) and hydrophilic (tween 80: HLB value 15; tween 60: HLB value 14.9; tween 40 HLB value 15.6; tween 20 HLB value 16.7) non-ionic surfactants; however, stable dispersions of MONCs were obtained exclusively with hydrophilic surfactants. Small volume fraction ($1/100^{th}$ of surfactant concentration) of cosurfactants aided in obtaining uniform dispersions of more hydrophobic hexameric formulations. Fig. 2 gives a pictorial model of a hexameric nanocapsule enclosed in a micelle.

Samples were prepared by mixing capsules with surfactants at (0.4 to 0.6) m^3/m^3 concentration (described as volume concentrations) and cosurfactants ≈(10 to 100) μl (*e.g.* butanol). The resultant co-complex was mixed with water, heated and sonicated to obtain a transparent micellar solution (Fig. 3). The dissolution of nanocapsules in water was confirmed by UV-vis spectroscopy experiments (ESI†) and the colour of aqueous solutions (Fig. 3). These micellar solutions of MONCs were then characterized by DLS and SANS measurements that yielded hydrodynamic radius (R_h) and radius of gyration (R_g) values, respectively. Both R_h and R_g represent the radius of the micelle; however, the R_h value for a given MONC is typically larger than R_g value, accounting for the viscosity drag at the surface of micelles. DLS yields the radius based on how fast micelles move in solvent, hence the name "dynamic" whereas SANS fit is a "static" fit, that is a snapshot (time-averaged) of the radius of scatterers. The scattering event happens on a much shorter time scale than the particles are moving, so it is "static".

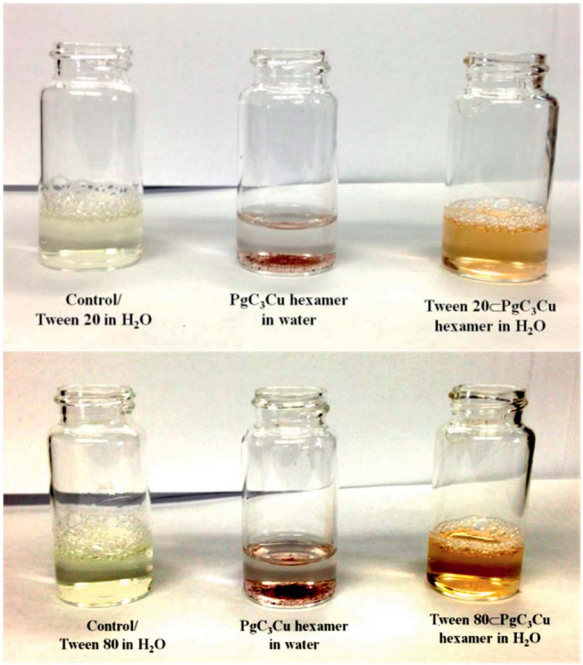

Fig. 3 Top: H_2O solubilized samples from left to right: tween 20 in H_2O, PgC_3Cu hexamer in H_2O, tween 20⊂PgC_3Cu hexamer in H_2O; bottom: H_2O solubilized samples from left to right tween 80 in H_2O, PgC_3Cu hexamer in H_2O, tween 80⊂PgC_3Cu hexamer in H_2O.

The control and surfactant-solubilized MONCs were centrifuged and filtered through 0.1 μm or 0.02 μm filters before DLS analysis. DLS is sensitive to dust particles, hence filtration is an essential step for light scattering measurements. The assays were performed at 20 °C with an acquisition time of 10 s and sensitivities of 10% and 50% on Dyna-Pro software for DLS measurements. Note that the sensitivity did not affect the quality of data. The SANS measurements were performed on the NG-3 SANS instrument at the NIST Center for Neutron Research, Gaithersburg, MD.[36] Of the various surfactant combinations utilized, polyoxyethylene (20) sorbitan monooleate, (C18:1; tween 80), polyoxyethylene (20) sorbitan monopalmitate, (C16:0; tween 40) and polyoxyethylene (20) sorbitan monolaurate, (C12:0; tween 20) provided stable solutions for $(PgC_3)_2M_8L_8$ dimers, where M = Zn, Co, Ni and $(PgC_3)_6Ni_{24}L_{24}$ and $(PgC_3)_6Cu_{24}$ hexamers (Fig. 4). The surfactant concentrations of 0.4 m^3/m^3 and 0.6 m^3/m^3 were used to solubilize dimers and hexamers, respectively, accounting for the higher hydrophobicity of hexamers. DLS studies were conducted on $(PgC_3)_6Cu_{24}$ hexamers and $(PgC_3)_2Zn_8L_8$ dimers whereas SANS measurements were conducted on $(PgC_3)_6Cu_{24}$ and $(PgC_3)_6Ni_{24}L_{24}$ hexamers and $(PgC_3)_2Ni_8L_8$ and $(PgC_3)_2Co_8L_8$ dimers. Similarities in overall metric dimensions of nanocapsules, irrespective of the type of metal involved, allow us to make appropriate comparisons between SANS and DLS measurements.[33,37,38]

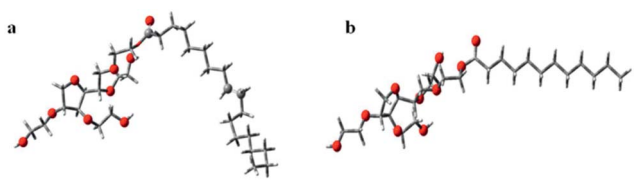

Fig. 4 (a) Tween 80 surfactant molecule showing its double bond at the C9 position and bent structure of the surfactant molecule; (b) tween 20 surfactant molecule. Color codes: C: grey; O: red; H: white.

The DLS measurements of aqueous solutions of hexamers and dimers yielded regularization histograms, representing the size distribution of the distinct, resolvable species or population of nanoparticles in solution. The regularization histogram of both $(PgC_3)_6Cu_{24}$ hexamers and $(PgC_3)_2Zn_8L_8$ dimers shows monomodal distributions, indicating the presence of single discrete micellar entity. At 0.6 m^3/m^3 surfactant concentrations, the R_h of tween 20⊂$(PgC_3)_6Cu_{24}$ micelle (r = 4.2 nm) is about 2 Å smaller than that of tween 40⊂$(PgC_3)_6Cu_{24}$ micelle (r = 4.4 nm). This can be attributed to the difference in the alkyl tail lengths of tween 20 (n = 12) and tween 40 (n = 16). Interestingly, the R_h of tween 80⊂$(PgC_3)_6Cu_{24}$ micelle (r = 3.8 nm) is smaller than that of tween 20/40⊂$(PgC_3)_6Cu_{24}$ micelle due to the unsaturation at *cis*-C9 position and the bent shape of the tween 80 (n = 18) surfactant molecule (Fig. 4; Table 1).

At lower surfactant concentrations of 0.4 m^3/m^3, stable solutions of hexamers are obtained with the aid of butanol cosurfactant (10 μl). The R_h for $(PgC_3)_6Cu_{24}$ micelles varied from 3.7 nm to 4.1 nm to 3.7 nm for tween 20, tween 40 and tween 80, respectively (Table 1; Fig. 2). Although similar trends in radius are observed at 0.4 m^3/m^3 and 0.6 m^3/m^3 surfactant concentrations, slight differences in R_h and molar masses are observed due to the presence of co-surfactant.

The number of pyrogallol[4]arene units in dimeric (2 arenes) *versus* hexameric (6 arenes) nanocapsules account for the lower hydrophobicity of dimers. Thus, the solution of $(PgC_3)_2Zn_8L_8$ dimeric micelles are much more easily stabilized in aqueous media at both 0.4 m^3/m^3 and 0.6 m^3/m^3 polysorbitan concentrations without the aid of cosurfactant. The DLS measurements of tween 20⊂$(PgC_3)_2Zn_8L_8$, tween 40⊂$(PgC_3)_2Zn_8L_8$ and tween 80⊂$(PgC_3)_2Zn_8L_8$ yielded R_h values of 3.8 nm, 4.0 nm and 3.7 nm at 0.4 m^3/m^3 and 3.8 nm, 4.2 nm and 3.6 nm at 0.6 m^3/m^3 surfactant concentrations, respectively (Table 1; ESI†). Note the trends of radius with respect to the alkyl tails of surfactants are similar for dimers and hexamers (Table 1).

Table 1 Hydrodynamic radius of water solubilised $(PgC_3)_6Cu_{24}$ hexamers and $(PgC_3)_2Zn_8L_8$ dimers

(A)	0.6 m^3/m^3	R_h (nm)	(B)	0.4 m^3/m^3	R_h (nm)
$(PgC_3)_6Cu_{24}$ hexamers					
1	Tween 20	4.24	1	Tween 20	3.68
2	Tween 40	4.44	2	Tween 40	4.05
3	Tween 80	3.79	3	Tween 80	3.77
$(PgC_3)_2Zn_8L_8$ dimers					
1	Tween 20	3.83	1	Tween 20	3.77
2	Tween 40	4.16	2	Tween 40	4.04
3	Tween 80	3.63	3	Tween 80	3.66

For SANS measurements, we used deuterated solvents to improve the contrast and to obtain coherent scattering, which possess the structural information. The control sample of surfactants and surfactant⊂$(PgC_3)_nM_{4n}L_{0-4n}$/nanocapsule were prepared in D_2O. Unlike the DLS measurements, we do not filter the samples for SANS studies and hence lower surfactant concentrations (0.2 m^3/m^3) are preferred to ensure no aggregation and to obtain good scattering statistics (ESI†). The micellar samples were filtered exclusively for DLS measurements to ensure (a) no dust particles/aggregates affect the autocorrelation curves and (b) expulsion of aggregates which may result at higher surfactant concentration. The filtration of higher surfactant concentrations for DLS measurements and use of lower concentration (without filtration) for SANS measurements aided in obtaining monodisperse solutions of nanocapsule enclosed micelles, confirmed by scattering measurements and UV spectroscopy.

The SANS data for the control samples of tween 20 and tween 80 in D_2O as well as tween 20⊂$(PgC_3)_2Co_8L_8$ (dimer), tween 20⊂$(PgC_3)_6Ni_{24}L_{24}$ (hexamer), tween 80⊂$(PgC_3)_2Ni_8L_8$ (dimer), tween 80⊂$(PgC_3)_6Ni_{24}L_{24}$ (hexamer, with external metal-cordinated ligands) and tween 80⊂$(PgC_3)_6Cu_{24}$ (hexamer, without external metal-coordinated ligands) in D_2O best fitted to the polydisperse core–shell hard sphere model (Table 2; Fig. 5; ESI†). The presence or absence of external ligands corresponds to the square planar and square pyramidal coordination environment on the metal centers (Fig. 1).

The average core radius (surfactant) of ≈1.2 nm and ≈1.5 nm and shell thickness (surfactant + D_2O) of ≈1.6 nm and ≈1.9 nm was observed for tween 20 and tween 80 micelles in D_2O, respectively. Thus, an overall radius (core + shell) of ≈2.8 nm and ≈3.4 nm exists for tween 20 and tween 80 control samples, respectively. Similarly, the scattering data fit for tween 20⊂$(PgC_3)_2Co_8L_8$ (dimer), tween 20⊂$(PgC_3)_6Ni_{24}L_{24}$ (hexamer), tween 80⊂ $(PgC_3)_2Ni_8L_8$ (dimer), tween 80⊂$(PgC_3)_6Cu_{24}$ (hexamer) and tween 80⊂$(PgC_3)_6Ni_{24}L_{24}$ (hexamer) micelles yielded the average core radius (nanocapsule + surfactant) of 1.7 nm, 2.4 nm, 1.9 nm, 2.4 nm and 2.9 nm, respectively, and a shell thickness of 1.6 nm, 1.3 nm, 1.7 nm, 1.7 nm and 1.7 nm, respectively. A progression in core + shell radius exists as a function of nanocapsule radius within the micelles. The overall diameter increases from 3.3 nm for a dimer to 3.7 for a hexamer for tween 20 based micelles, whereas it changes from 3.2 nm for a dimer to 4.1 nm for $(PgC_3)_6Cu_{24}$ hexamer (without ext. ligands) to 4.6 nm for a $(PgC_3)_6Ni_{24}L_{24}$ hexamer (with ext. ligands) for tween 80 based micelles.

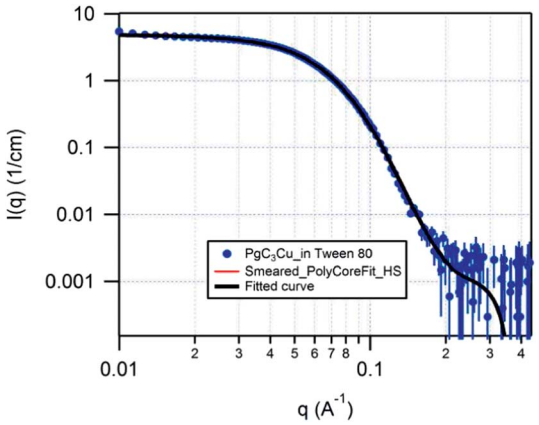

Fig. 5 Small-angle neutron scattering (SANS) data fit (polydisperse core–shell hard sphere fit) of tween⊂PgC_3Cu hexamer in D_2O. The blue points are the SANS data points, the red line is the smeared model curve (underneath the black curve: not visible) and the black line is the fitted curve. The error bars on the SANS data represent one standard deviation.

Nanocapsules solubilized in tween 20: SANS *vs.* DLS

The DLS results indicate an increase in the radius of the micelle with an increase in the radius of template/nanocapsule enclosed. Specifically, the radius varies from 3.5 nm to 3.8 nm to

Table 3 SANS and DLS result summary of $(PgC_3)_nM_{4n}L_{0-4n}$ nanocapsule-enclosed micelles in D_2O (tween 20)

Tween 20 DLS *versus* SANS result summary				
		R (nm)	R_g (nm)	R_g/R_h
DLS	Blank tween 20	$R_h = 3.5$		
SANS	Blank tween 20	$R_{HS} = 2.8$	2.16	0.62
DLS	Tween 20 ⊂$(PgC_3)_2Zn_8L_8$ dimer	$R_h = 3.8$		
SANS	Tween 20 ⊂$(PgC_3)_2Co_8L_8$ dimer	$R_{HS} = 3.3$	2.54	0.67
DLS	Tween 20 ⊂$(PgC_3)_6Cu_{24}$ hexamer	$R_h = 4.24$		
SANS	Tween 20 ⊂$(PgC_3)_6Ni_{24}$ hexamer	$R_{HS} = 3.8$	2.90	0.68

Table 2 SANS result summary of polydisperse core–shell sphere model of $(PgC_3)_nM_{4n}L_{0-4n}$ nanocapsule-enclosed micelles in D_2O (tween 20 and tween 80)

Sample	Co-surfactant	Core radii (nm)	Shell thickness (nm)	Core with shell (nm)	Chi-sqrt
Tween 20	Acetone	1.204	1.635	2.839	6.2
Tween 20	Acetonitrile	1.229	1.601	2.830	6.5
Tween 20	Isopropanol	1.206	1.611	2.817	5.8
Tween 20⊂$(PgC_3)_2Co_8L_8$ dimer	Isopropanol	1.704	1.662	3.366	1.5
Tween 20⊂$(PgC_3)_6Ni_{24}L_{24}$ hexamer	Acetonitrile	2.466	1.295	3.761	2.5
Tween 80	DMSO	1.542	1.988	3.530	9.2
Tween 80⊂$(PgC_3)_6Cu_{24}$ hexamer (without ligands)	None	2.409	1.726	4.135	2.6
Tween 80⊂$(PgC_3)_2Ni_8L_8$ dimer	DMSO	1.937	1.700	3.637	3.7
Tween 80⊂ $(PgC_3)_6Ni_{24}L_{24}$ hexamer (with ligand)	DMSO	2.902	1.654	4.556	5.5

Table 4 SANS and DLS result summary of PgC_3M nanocapsule-enclosed micelles in D_2O (tween 80)

Tween 80 DLS *versus* SANS result summary				
		R (nm)	R_g nm	R_g/R_h
DLS	Blank tween 80	$R_h = 3.27$		
SANS	Blank tween 80	$R_{HS} = 3.53$	2.72	0.83
DLS	Tween 80$\subset(PgC_3)_2Zn_8L_8$ dimer	$R_h = 3.63$		
SANS	Tween 80$\subset(PgC_3)_2Ni_8L_8$ dimer	$R_{HS} = 3.60$	2.77	0.76
DLS	Tween 80$\subset(PgC_3)_6Cu_{24}$ hexamer	$R_h = 3.78$		
SANS	Tween 80$\subset(PgC_3)_6Cu_{24}$ hexamer	$R_{HS} = 4.14$	3.19	0.84
SANS	Tween 80$\subset(PgC_3)_6Ni_{24}L_{24}$ hexamer with ligands	$R_{HS} = 4.56$	3.51	0.93

4.2 nm (at 0.6 m^3/m^3) for control/tween 20 to tween 20$\subset(PgC_3)_2Zn_8L_8$ dimer to tween 20$\subset(PgC_3)_6Cu_{24}$ hexamer, respectively, in water. The difference between the diameter of a micelle and a micelle with a dimer is about 0.6 nm while that for a hexamer is about 1.4 nm. This increase in diameter is smaller than the expected 1.8 nm diameter of $(PgC_3)_2Zn_8L_8$ dimer + micelle and 2.0 nm diameter of a $(PgC_3)_6Cu_{24}$ hexamer + micelle (from SANS);[33,35] however, the observed increase can be explained based on the fact that the micelles are formed with/without the template nanocapsule (Table 3).

It is important to note the SANS data analysis of a typical $(PgC_3)_2Cu_8$/$(PgC_3)_2Ni_8$ dimer (without ligands), $(PgC_3)_2Zn_8L_8$ dimer (with ligands), and $(PgC_3)_6Cu_{24}$ hexamer in acetone–methanol–DMSO yields a radius of 0.7 nm, 0.9 nm and 1.0 nm, respectively.[33,35] The solid-state structure of all dimers indicate the presence of external ligands; however, the only zinc-seamed framework retain the external ligands in DMSO solvent.[33,35] Hence, the radius of $(PgC_3)_2Zn_8L_8$ dimer is uniquely higher in non-polar solvent by about 2 Å than that of $(PgC_3)_2$ Cu_8/$(PgC_3)_2Ni_8$ dimers. Note that the overall framework of dimers is stable in solution and gas phases, with and without external ligands.[33,35]

Similar to the DLS measurements, the SANS measurements reveal an increase in the radius of an empty micelle from $r = 2.8$ nm to that of a dimer $r = 3.3$ nm to that of a hexamer $r = 3.8$ nm for a polycore_HS model (Table 3; ESI†). This difference in radius (between SANS empty *versus* dimeric micelles) of 0.5 nm for the dimer is smaller than the expected (0.7 to 0.9) nm radius difference and it indicates that there is a fractional change in the mean radius of a sphere when a comparatively smaller dimeric nanocapsule occupies the center of the cavity of the micelle. On the contrary, the radius difference of ≈1.0 nm between SANS empty *versus* hexameric micelles is similar to the 1.0 nm radius of hexamers (in DMSO). Radius of gyration (R_g) values obtained from the static radius values (R_{HS}) yield similar trends in radius dimensions ($R_g = 0.77 \times R_{HS}$; Table 3).

Comparing the DLS (R_h) *vs.* SANS (R_{HS}) radius values, we get a difference of 0.7, 0.5 and 0.5 nm between R_{HS} and R_h for the blank, dimeric and hexameric samples, respectively (Table 3). The R_g/R_h ratio ≈0.77 (Table 3) indicate the sphericity of micelles and the presence of a large solvent sheath around the micelles. The solvent sheath can be attributed to the high HLB value for tween 20 (16.7) and close association of surfactant polar head groups with water. Interestingly, the difference in radius between the dimer-enclosed micelle and hexamer-enclosed micelle is 0.47 nm on DLS and 0.46 nm on SANS that is close to the observed difference in R of 0.48 nm (with ligands on a hexamer) between the dimers and the hexamers themselves.

Nanocapsules solubilized in tween 80: SANS *vs.* DLS

Similar to the tween 20 solubilization experiments, the DLS measurements and data analysis of tween 80 samples reveal an increase in radius of the micelles of tween 80 ($r = 3.3$ nm) to that of the tween 80$\subset(PgC_3)_2Zn_8$ dimer ($r = 3.6$ nm) and to that of tween 80$\subset(PgC_3)_6Cu_{24}$ hexamer ($r = 3.8$ nm), at 0.6 m^3 m^{-3} concentration. The difference between the diameter of a micelle and tween 80$\subset(PgC_3)_2Zn_8L_8$ dimer is about 0.72 nm and that with hexamer is about 1.02 nm. This increase in diameter is smaller by about 6 Å than with tween 20 solubilization; nonetheless, it can be explained based on the fact that the micelles of tween 80 have bent hydrophobic tails at carbon length C9 interacting with the alkyl chains of the nanocapsules, whereas tween 20 has an elongated straight chain of 12 carbon atoms (Fig. 4). The bent structure of the chains could reasonably account for the differences in size of the nanocapsule-enclosed micelles in the two surfactants (Table 4).

In contrast to the average R_g/R_h ratio of ≈0.7 for the tween 20 blank samples, the tween 80 blank samples ($r = 3.44$ nm) show an increase in the R_g/R_h ratio > 0.77 indicative of less compact species. A possible explanation for this result is the inability of tween 80 molecules to organize in a compact uniform micellar arrangement due to the bent shape of the alkyl tails from unsaturation at the C9 position (Fig. 4). Furthermore, the SANS measurements reveal an increase in the radius of micelles of tween 80$\subset(PgC_3)_2Ni_8L_8$ dimer (r = 3.6 nm) to tween 80$\subset(PgC_3)_6Cu_{24}$ hexamer-without external ligands (r = 4.14 nm) to tween 80$\subset(PgC_3)_6Ni_{24}L_{24}$ hexamer-with external ligands ($r = 4.56$ nm). This increase in radius suggests templation and corresponding rearrangement of the surfactant (tween 80) or possible reduction in aggregation number of surfactant around the nanocapsules (Table 4).

Conclusions

In conclusion, commercially available non-ionic surfactants (polysorbitans/tweens) are efficient in facilitating the solubilization of MONCs ($(PgC_3)_6Cu_{24}$, $(PgC_3)_6Ni_{24}L_{24}$, $(PgC_3)_2Ni_8L_8$, $(PgC_3)_2Zn_8L_8$, $(PgC_3)_2Co_8L_8$) in water. *In situ* scattering measurements reveal an increase in the radius of the micelles with an increase in the length of the alkyl tails of surfactants (tween 20, C12 *vs.* tween 40, C16) or

with an increase in radius of the nanocapsule (hexamer *vs.* dimer). In contrast, tween 80 (C18:1, 9) though with long alkyl chain length, forms comparatively smaller-sized micelles (given the longer alkyl tail of surfactants) owing to the presence of a double bond at the C9 position in the alky tail and the bent structure of the surfactant. Combined DLS and SANS data analyses of tween 20 based micelles yield the ratios of radius of gyration to hydrodynamic radius (R_g/R_h) of $\approx$0.7, demonstrating the spherical nature of micelles in solution. The lower ratios of R_g/R_h for tween 20 based micelles *versus* tween 80 based micelles clearly indicate the effect of the shape of surfactant in governing the architecture and compactness of micelles in solution. The solution studies conducted herein presents, for the first time, complex fluids of nanocapsules with surfactants. Future studies will focus on temperature and shear effects to further investigate their material properties.

Acknowledgements

We thank NSF for support of this work (J.L.A). This work utilized facilities supported in part by the National Science Foundation under Agreement no. DMR-0944772 (S.R.K.), NSF grant CHE-89-08304. Certain trade names and company products are identified to adequately specify the experimental procedure. In no case does such identification imply recommendation or endorsement by the National Institute of Standards and Technology, nor does it imply that the products are necessarily best for the purpose. We also thank Prof. Carol A. Deakyne for valuable discussions.

Notes and references

1 C. Wang, E. Wyn-Jones, J. Sidhu and K. C. Tam, *Langmuir*, 2007, **23**, 1635–1639.
2 Z. Zhang, Y. Luo, B. Xia, C. Han, Y. Yu, X. Chen and F. Huang, *Chem. Commun.*, 2011, **47**, 2417.
3 C. Han, F. Ma, Z. Zhang, B. Xia, Y. Yu and F. Huang, *Org. Lett.*, 2010, **12**, 4360–4363.
4 Z. Zhang, B. Xia, C. Han, Y. Yu and F. Huang, *Org. Lett.*, 2010, **12**, 3285–3287.
5 Y. Zhou, C. Liu, H. Xu, H. Yu, Q. Lu and L. Wang, *Spectrochim. Acta, Part A*, 2007, **66A**, 919–923.
6 X. Ji, J. Li, J. Chen, X. Chi, K. Zhu, X. Yan, M. Zhang and F. Huang, *Macromolecules*, 2012, **45**, 6457–6463.
7 P. K. Singh, M. Kumbhakar, R. Ganguly, V. K. Aswal, H. Pal and S. Nath, *J. Phys. Chem. B*, 2010, **114**, 3818–3826.
8 P. K. Singh, M. Kumbhakar, H. Pal and S. Nath, *J. Phys. Chem. B*, 2008, **112**, 7771–7777.
9 P. K. Singh, M. Kumbhakar, H. Pal and S. Nath, *J. Phys. Chem. B*, 2009, **113**, 1353–1359.
10 A. Spagnul, C. Bouvier-Capely, M. Adam, G. Phan, F. Rebiere and E. Fattal, *Int. J. Pharm.*, 2010, **398**, 179–184.
11 A. W. Coleman, C. Mbemba, P. Falson, R. Matar, F. Huche, *FR Pat.*, 2931695, 2009.
12 K. S. J. Iqbal, M. C. Allen, F. Fucassi and P. J. Cragg, *Chem. Commun.*, 2007, 3951–3953.
13 P. Jin, S. J. Dalgarno, C. Barnes, S. J. Teat and J. L. Atwood, *J. Am. Chem. Soc.*, 2008, **130**, 17262–17263.
14 P. Jin, S. J. Dalgarno, J. E. Warren, S. J. Teat and J. L. Atwood, *Chem. Commun.*, 2009, 3348–3350.
15 H. Kumari, S. R. Kline, W. Wycoff, R. L. Paul, A. V. Mossine, C. A. Deakyne and J. L. Atwood, *Angew. Chem.*, 2012, **51**, 5086–5091.
16 R. M. McKinlay, P. K. Thallapally and J. L. Atwood, *Chem. Commun.*, 2006, 2956–2958.
17 R. M. McKinlay, P. K. Thallapally, G. W. V. Cave and J. L. Atwood, *Angew. Chem.*, 2005, **44**, 5733–5736.
18 S. J. Dalgarno, S. A. Tucker, D. B. Bassil and J. L. Atwood, *Science*, 2005, **309**, 2037–2039.
19 D. B. Bassil, S. J. Dalgarno, G. W. V. Cave, J. L. Atwood and S. A. Tucker, *J. Phys. Chem. B*, 2007, **111**, 9088–9092.
20 S. J. Dalgarno, D. B. Bassil, S. A. Tucker and J. L. Atwood, *Angew. Chem., Int. Ed.*, 2006, **45**, 7019–7022.
21 K. K. Kline, D. A. Fowler, S. A. Tucker and J. L. Atwood, *Chem.–Eur. J.*, 2011, **17**, 10848–10851.
22 J. L. Whetstine, K. K. Kline, D. A. Fowler, C. M. Ragan, C. L. Barnes, J. L. Atwood and S. A. Tucker, *New J. Chem.*, 2010, **34**, 2587–2591.
23 H. Kumari, S. R. Kline and J. L. Atwood, *Chem. Commun.*, 2012, **48**, 3599.
24 S. J. Dalgarno, N. P. Power and J. L. Atwood, *Coord. Chem. Rev.*, 2008, **252**, 825–841.
25 R. W. Saalfrank, H. Glaser, B. Demleitner, F. Hampel, M. M. Chowdhry, V. Schunemann, A. X. Trautwein, G. B. M. Vaughan, R. Yeh, A. V. Davis and K. N. Raymond, *Chem.–Eur. J.*, 2002, **8**, 493–497.
26 T. McMurry, K. Raymond and P. Smith, *Science*, 1989, **244**, 938–943.
27 D. W. Johnson and K. N. Raymond, *Inorg. Chem.*, 2001, **40**, 5157–5161.
28 D. L. Caulder, R. E. Powers, T. N. Parac and K. N. Raymond, *Angew. Chem., Int. Ed.*, 1998, **37**, 1840–1843.
29 N. Takeda, K. Umemoto, K. Yamaguchi and M. Fujita, *Nature*, 1999, **398**, 794–796.
30 K. Suzuki, M. Kawano and M. Fujita, *Angew. Chem., Int. Ed.*, 2007, **46**, 2819–2822.
31 R. L. Paul, S. P. Argent, J. C. Jeffery, L. P. Harding, J. M. Lynam and M. D. Ward, *Dalton Trans.*, 2004, 3453–3458.
32 S. P. Argent, H. Adams, L. P. Harding and M. D. Ward, *Dalton Trans.*, 2006, 542–544.
33 H. Kumari, A. V. Mossine, S. R. Kline, C. L. Dennis, D. A. Fowler, S. J. Teat, C. L. Barnes, C. A. Deakyne and J. L. Atwood, *Angew. Chem.*, 2012, **51**, 1452–1454.
34 H. Kumari, S. R. Kline, N. J. Schuster and J. L. Atwood, *Chem. Commun.*, 2011, **47**, 12298.
35 D. A. Fowler, A. S. Rathnayake, S. Kennedy, H. Kumari, C. M. Beavers, S. J. Teat and J. L. Atwood, *J. Am. Chem. Soc.*, 2013, **135**, 12184–12187.
36 C. J. Glinka, J. G. Barker, B. Hammouda, S. Krueger, J. J. Moyer and W. J. Orts, *J. Appl. Crystallogr.*, 1998, **31**, 430–445.
37 R. M. McKinlay, G. W. V. Cave and J. L. Atwood, *Proc. Natl. Acad. Sci. U. S. A.*, 2005, **102**, 5944–5948.
38 J. L. Atwood, E. K. Brechin, S. J. Dalgarno, R. Inglis, L. F. Jones, A. Mossine, M. J. Paterson, N. P. Power and S. J. Teat, *Chem. Commun.*, 2010, **46**, 3484–3486.